14th International Symposium on Turbulence and Shear Flow Phenomena (TSFP14)
Heidelberg, Germany, July 28–31, 2026

TURBULENT FLOW OF A CHANNEL BOUNDED BY A SINUSOIDAL HYPER-ELASTIC WALL

M. S. Aswathy
Department of Aerospace Engineering
Indian Institute of Space Science and Technology
Thiruvananthapuram, Kerala 695547, India
aswathyms@iist.ac.in

Morie Koseki
Complex Fluids and Flows Unit
Okinawa Institute of Science and Technology
1919-1 Tancha, Onna-son, Kunigami-gun,
Okinawa 904-0495, Japan
MORIE.KOSEKI@OIST.JP

Marco Edoardo Rosti
Complex Fluids and Flows Unit
Okinawa Institute of Science and Technology
1919-1 Tancha, Onna-son, Kunigami-gun,
Okinawa 904-0495, Japan
MARCO.ROSTI@OIST.JP

ABSTRACT

We perform Direct Numerical Simulations to understand the turbulent flow statistics and dynamics of a channel bounded by an incompressible viscous hyper-elastic wall (modeled as a neo-Hookean material obeying the Mooney-Rivlin law), having a sinusoidal shape in its unstressed state. The simulations are carried out at a bulk Reynolds number 2800, and we examine the influence of different values of the initial wall amplitudes on the flow statistics and wall deformations. Among the tested cases, we observe that the friction Reynolds number exhibits a non-monotonic trend with respect to increasing amplitude: at a specific value, the friction Reynolds number drops compared to the baseline case, and beyond that, it starts rising again. The study explores the drag increase/reduction mechanism using different statistical measures and probing near-wall structures.

INTRODUCTION

Understanding the prospective impact of material compliance on turbulent flow has attracted attention to both fundamental and industrial problems; for example, laminar-to-turbulent transition delay (e.g., Nagy *et al.* (2022)), and friction drag reduction (e.g., Gad-el Hak (2002)). The use of compliant surfaces to flow control is particularly intriguing in a class of wall-bounded flows, due to its passive nature requiring no additional energy (Tian *et al.*, 2021).

The early research on compliant walls were limited to theoretical investigations, due to the complexity of the problem arising from the mutual interaction between the deformable walls and turbulence. In particular, there was an interest to identify possible delays in transition and attenuation of turbulence (Kumaran, 2021). However, wall compliance can lead to both flow stabilization and destabilization (e.g., Benjamin (1960, 1963); Landahl (1962)). Compliant walls can stabilize the Tollmien-Schlichting instability, thereby delaying transition, but compliant walls can also experience surface destabilizations, inducing new instabilities (Davies & Carpenter, 1997b,a). The theoretical work has recently been extended to interactions with turbulent flows, reporting that pressure instabilities lead to a larger-amplitude surface wave whose variations are characterized by the material properties (Duncan, 1986; Benschop *et al.*, 2019).

In the experimental investigations, the literature reported two different coupling motions between compliant walls and turbulent flows. When wall deformation is smaller than one wall unit, the system is called one-way coupled, where a traveling wave is observed, which correlates with turbulent pressure fluctuations (Zhang *et al.*, 2015, 2017). On the other hand, when the complaint wall deforms more than several wall units, the system is called two-way coupled, where it emerges that the streamwise-aligned wave travels in the spanwise direction, and the spanwise-aligned wave travels in the streamwise direction (Wang *et al.*, 2020; Greidanus *et al.*, 2022).

In early numerical studies, compliant walls were modeled as simplified mass-spring-damper systems (Endo & Himeno, 2002; Kim & Choi, 2014). Only recently have direct numerical simulations been able to fully resolve fluid-structure interaction in turbulent flows. The presence of the compliant wall has been shown to increase the drag significantly due to the enhancement of the wall-normal fluctuation, leading to a decay in the streamwise coherent structures and increased spanwise coherency (Rosti & Brandt, 2017). These spanwise coherent structures bring high-speed momentum flow towards the compliant wall, which reacts with intense ejection events (Ardekani *et al.*, 2019). This is caused by the negative vorticity lifting up, which is enhanced when the advection speed of near-wall pressure fluctuations matches the phase speed of Rayleigh waves (Esteghamatian *et al.*, 2022). This indicates that wave propagation within or above the compliant wall can also increase turbulent intensity (Wang *et al.*, 2020). Additionally, the above effects cannot be fully attributed to the wall deformation, and the wall compliance itself affects turbulent flows (Koseki *et al.*, 2025).

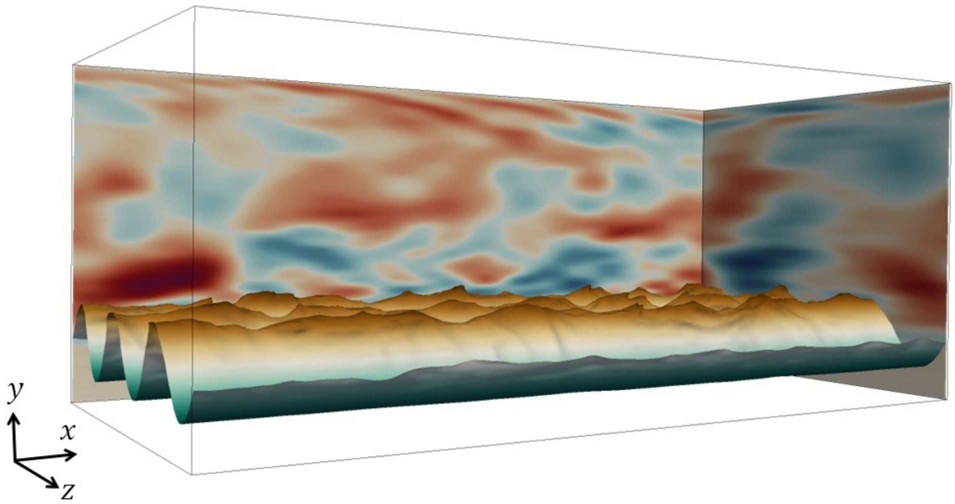

Figure 1. Visualization of the computational domain with the fluid occupying the region above the wavy interface, and the viscous hyper-elastic solid occupying the region below the interface. The interface surface is colored from green (negative) to orange (positive), indicating the wall elevation with respect to a flat interface. The side panels show the instantaneous streamwise velocity fluctuations (colored from blue (negative) to red (positive).

Previous research has mainly examined the effects of compliant walls starting from a horizontal equilibrium position. However, the effects of the initial surface shape on the compliant wall have not yet been widely studied. In this work, we thus study turbulent channel flows bounded by a compliant wall with a wavy shape in its unstressed state. We aim to understand how the magnitude of its initial amplitude influences the turbulent statistics and flow dynamics inside the channel.

NUMERICAL METHOD

An incompressible fluid flowing through a channel with an incompressible viscous hyper-elastic wall is considered. Direct numerical simulations are performed on a configuration wherein the channel is bounded by a rigid wall and a sinusoidal compliant wall at the bottom, which is spatially periodic in the spanwise direction, as shown in Figure 1. The incompressibility constraints and the momentum equations govern both the fluid and the solid phases, where the Cauchy stress tensors are either that of a Newtonian fluid or of a neo-Hookean solid (Bonet & Wood, 2008). The fluid-structure interaction problem is solved through a one-continuum formulation based on the volume-of-fluid method, with the continuity of velocity and traction forces enforced at the interface between the two phases. Finally, to close the equations using the Eulerian formulation, we also solve the transport equation for the solid volume fraction and the left Cauchy–Green deformation tensor (Sugiyama *et al.*, 2011). To solve this system numerically, the second-order central finite-difference scheme is applied as the space discretization, except for a WENO scheme applied to the advection terms in the transport equations. The rest of the system is advanced in time by the third-order Runge-Kutta scheme, with the Crank-Nicolson scheme used for the solid stress term in the Cauchy stress equation. The details of the formulation and numerical methods are provided in Rosti & Brandt (2017).

RESULTS and DISCUSSION

We study turbulent channel flows over compliant walls with a wavy interface, along with flat-interface walls as a reference case. All cases are performed at a constant flow rate, and analysis is done when the pressure gradient is statistically converged. The bulk Reynolds number $Re_b = 2800$ (based on the bulk velocity U_b and the half channel height h) and the modulus of transverse elasticity of the wall $G = 1.0\rho U_b^2$ are kept fixed, and only the amplitude of the sinusoidal wall geometry is varied here. Under unstressed conditions, the amplitude is varied from a/h = 0.0 (corresponding to a flat interface) to a/h = 0.25.

Figure 2 shows the variation of the friction Reynolds number Re_τ on the hyper-elastic wall with a parametric variation in the amplitude a/h, and the figure shows a non-monotonic trend with respect to the variation of the amplitude. In fact, there is a specific value of the wall amplitude that shows a minimum Re_τ within the cases considered. Beyond this amplitude, Re_τ increases further with an increase in wall amplitude.

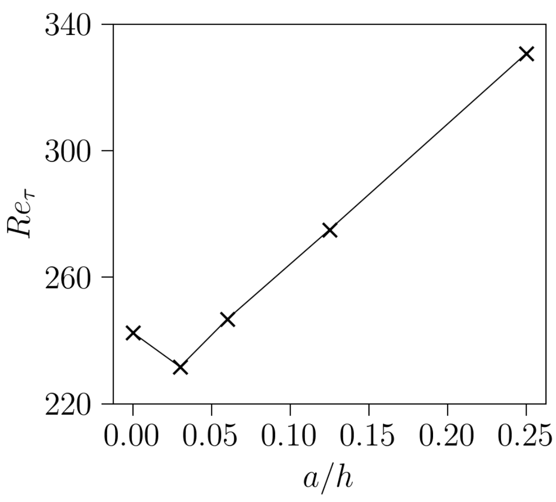

Figure 2. Variation of the friction Reynolds number with the amplitude of the sinusoidal compliant wall.

To understand this non-monotonic trend in the overall drag, we next look at the stress balance contributions integrated across the wall-normal direction. In the turbulent channel flow over compliant walls, the mean momentum balance can be described as:

$$\tau_w = \tau_V + \tau_R + \tau_E. \tag{1}$$

Here, τ_w is the total stress, which can be decomposed into the three terms shown in the right-hand side: the first term is the viscous stress τ_V, the second term is the Reynolds shear stress τ_R, and the third term is the contribution from the hyper-elastic wall τ_E. However, since the surface geometry is not homogeneous along the spanwise direction, as shown in Figure 1, we need to extend this formulation to account for the wavy shape of the compliant wall. To do so, we consider averages only in time and in space, with the latter being limited to the only homogeneous direction, i.e., the streamwise direction. Thus, the velocity $\mathbf{u}(x,y,z,t)$ is decomposed into a mean $\langle \mathbf{u} \rangle (y,z)$, where $\langle \cdot \rangle$ indicates average in the streamwise direction and time, and a fluctuations $\mathbf{u}'(x,y,z,t)$, i.e.,

$$\mathbf{u}(x,y,z,t) = \langle \mathbf{u} \rangle (y,z) + \mathbf{u}'(x,y,z,t). \tag{2}$$

This decomposition can capture the spatial inhomogeneity caused by the wall shape more effectively than the classical Reynolds decomposition. Introducing this decomposition into the momentum equation along the streamwise direction, results in the following relation:

$$\begin{aligned}
\tau_w(y-H) = & \underbrace{\int_H^y \mu \frac{\partial^2 \langle u \rangle}{\partial y^2} dy}_{\tau_V} \\
& \underbrace{- \int_H^y \mu \frac{\partial^2 \langle u \rangle}{\partial z^2} dy}_{\tau_{V_{inh}}} \\
& \underbrace{+ \int_H^y \rho \left\langle \frac{\partial u'v'}{\partial y} \right\rangle dy}_{\tau_R} \\
& \underbrace{+ \int_H^y \rho \left\langle \frac{\partial u'u'}{\partial x} \right\rangle dy + \int_H^y \rho \left\langle \frac{\partial u'w'}{\partial z} \right\rangle dy}_{\tau_{R_{inh}}} \\
& \underbrace{- \int_H^y G \left\langle \frac{\partial B_{xy}}{\partial y} \right\rangle dy}_{\tau_E} \\
& \underbrace{- \int_H^y G \left\langle \frac{\partial B_{xx}}{\partial x} \right\rangle dy - \int_H^y G \left\langle \frac{\partial B_{xz}}{\partial z} \right\rangle dy}_{\tau_{E_{inh}}} \\
& \underbrace{+ \int_H^y \rho \langle v \rangle \frac{\partial \langle u \rangle}{\partial y} dy + \int_H^y \rho \langle w \rangle \frac{\partial \langle u \rangle}{\partial z} dy,}_{\tau_A}
\end{aligned} \tag{3}$$

where $H = 2.5h$ is the total vertical length of the domain, μ the dynamic viscosity, ρ the density (μ and ρ are the same in both the fluid and solid phases), and B the left Cauchy-Green deformation tensor. Here, $\tau_{V_{inh}}$, $\tau_{R_{inh}}$, $\tau_{E_{inh}}$, and τ_A represent the contribution from the viscous diffusion, Reynolds stress, solid stress from hyper-elastic wall, and advection -all of them, caused by the presence of spanwise inhomogeneity.

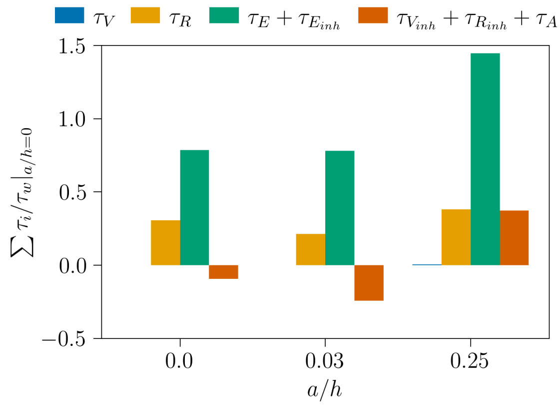

Figure 3. The integral contribution of the different stress components introduced in Eq. (3) across the wall-normal direction. Each color bar represents the different contributions to the total shear stress: viscous stress (blue), Reynolds shear stress (orange), total solid stress from compliant wall (green), and the other stress terms caused by the inhomogeneous geometry (red).

Figure 3 shows the integral shear stress balance contributions as a function of the wall-normal direction for three representative cases: baseline ($a/h = 0.0$), drag reduction ($a/h = 0.03$), and drag increase ($a/h = 0.25$), which also displays the non-monotonic trend observed in Figure 2. The figure clarifies that, among the different contributions, the solid stress is predominantly responsible for the total shear stress, i.e., the total drag. As the amplitude increases, the compliant wall contribution grows substantially, as does the Reynolds shear stress, while the viscous stress contribution is canceled out by integration over the full domain. The contribution from geometrical inhomogeneity seems to enhance the drag decrease/increase, with further analysis needed to disentangle this effect. Compared to the baseline, the drag-increase case shows all stress components are strengthened, leading to larger total stress, whereas the drag-reduction case shows comparable solid stress, slightly smaller Reynolds shear stress, and larger negative geometrical inhomogeneous contributions that help reduce the total shear stress.

The above observations are also apparent in the turbulent structures and in the hyper-elastic wall deformations. Figure 4 shows instantaneous snapshots for the contour surfaces of the streamwise velocity fluctuations and the bottom compliant wall. In the baseline case, the streamwise fluctuations are elongated in the spanwise direction, and the wall deformation aligned along the streamwise direction, as reported by Rosti & Brandt (2017); Koseki *et al.* (2025). Compared to the baseline, the drag-reduction case shows small, fragmented structures and fine wall undulations with a multitude of small-scale features, indicating reduced stress from both turbulent flows and the compliant wall. On the other hand, in the drag-increased case, the structures become larger, and the sinusoidal wall deforms at the top and sides, which corresponds to the larger

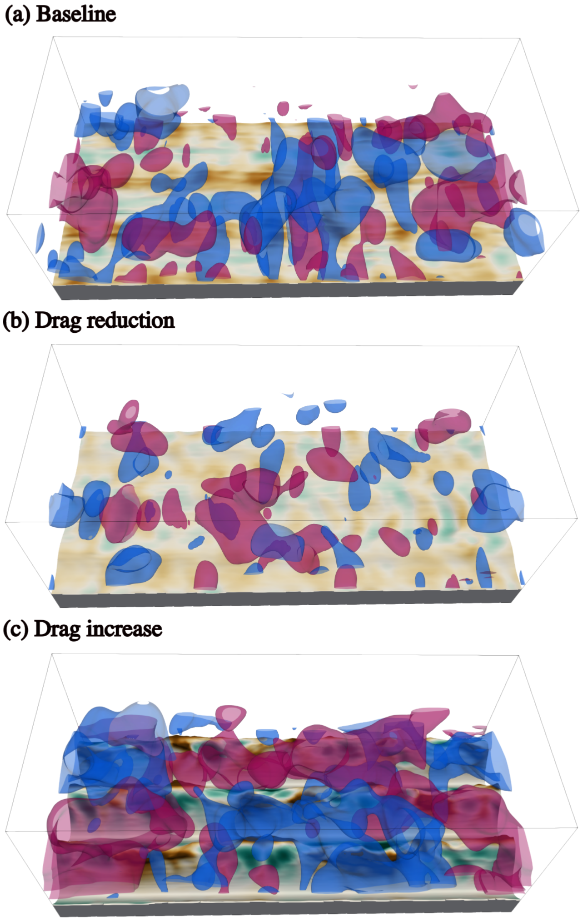

Figure 4. The instantaneous turbulent structures and deformation of the compliant wall for the (a) baseline, (b) drag reduction, and (c) drag increase cases, same as Figure 3. The iso-surfaces correspond to the streamwise velocity fluctuations between the channel center and the bottom compliant wall: $u' = 0.1$ (red) and -0.1 (blue). The surface interface is colored by the wall displacement from its equilibrium position, with the range from $-0.08h$ (green) to $0.08h$ (orange).

Reynolds shear stress and the significantly strengthened solid wall stress of the compliant wall. In general, the size of the turbulent structures and the deviation of the wall deformation tend to increase when the drag increases, which is also consistent with the trend of shear stress, as shown in Figure 3, confirming that the initial shape of the compliant walls can affect turbulent flows through the interaction of the dynamics of the wall and turbulent structures, thus reducing/strengthening the drag.

CONCLUSION

In this work, we study the turbulent dynamics and statistics of a channel with sinusoidal viscous hyper-elastic walls. We find that variations in the amplitude of the compliant wall have a significant impact on turbulent statistics and flow dynamics. It is seen that increasing the amplitude of the compliant wall increases the drag in general; however, there exists a specific amplitude of the wall geometry at which there is a reduction in friction. This non-monotonic trend is also observed in the integrated shear stress balance, with the effects of the inhomogeneous geometry introduced. The hyper-elastic solid stress contributes a significant portion of the total shear stress, and the Reynolds stress also increases drag; however, the geometric inhomogeneous contributions need more discussion. Finally, we look at instantaneous turbulent structures and wall deformations, which show that, compared to baseline, smaller turbulent structures and wall deformations are observed in the drag-reduction case, while larger ones are observed in the drag-increase case. These results suggest that the initial amplitude height affects the turbulent structures and wall dynamics, resulting in the drag changes.

REFERENCES

Ardekani, M. N., Rosti, M. E. & Brandt, L. 2019 Turbulent flow of finite-size spherical particles in channels with viscous hyper-elastic walls. *Journal of Fluid Mechanics* **873**, 410–440.

Benjamin, T Brooke 1960 Effects of a flexible boundary on hydrodynamic stability. *Journal of Fluid Mechanics* **9** (4), 513–532.

Benjamin, T Brooke 1963 The threefold classification of unstable disturbances in flexible surfaces bounding inviscid flows. *Journal of Fluid Mechanics* **16** (3), 436–450.

Benschop, HOG, Greidanus, AJ, Delfos, R, Westerweel, J & Breugem, W-P 2019 Deformation of a linear viscoelastic compliant coating in a turbulent flow. *Journal of Fluid Mechanics* **859**, 613–658.

Bonet, Javier & Wood, Richard D. 2008 *Nonlinear Continuum Mechanics for Finite Element Analysis*, 2nd edn. Cambridge University Press.

Davies, Christopher & Carpenter, Peter W 1997a Instabilities in a plane channel flow between compliant walls. *Journal of Fluid Mechanics* **352**, 205–243.

Davies, Christopher & Carpenter, Peter W 1997b Numerical simulation of the evolution of tollmien–schlichting waves over finite compliant panels. *Journal of Fluid Mechanics* **335**, 361–392.

Duncan, James H 1986 The response of an incompressible, viscoelastic coating to pressure fluctuations in a turbulent boundary layer. *Journal of Fluid Mechanics* **171**, 339–363.

Endo, Takahide & Himeno, Ryutaro 2002 Direct numerical simulation of turbulent flow over a compliant surface. *Journal of Turbulence* **3** (1), 007.

Esteghamatian, Amir, Katz, Joseph & Zaki, Tamer A. 2022 Spatiotemporal characterization of turbulent channel flow with a hyperelastic compliant wall. *Journal of Fluid Mechanics* **942**, A35.

Greidanus, A.J., Delfos, R., Picken, S.J. & Westerweel, J. 2022 Response regimes in the fluid-structure interaction of wall turbulence over a compliant coating. *Journal of Fluid Mechanics* **952**, A1.

Gad-el Hak, Mohamed 2002 Compliant coatings for drag reduction. *Progress in Aerospace Sciences* **38** (1), 77–99.

Kim, Euiyoung & Choi, Haecheon 2014 Space–time characteristics of a compliant wall in a turbulent channel flow. *Journal of fluid mechanics* **756**, 30–53.

Koseki, Morie, Aswathy, MS & Rosti, Marco Edoardo 2025 Understanding the effect of wall elasticity in turbulent channel flows. *Journal of Fluid Mechanics* **1021**, A4.

Kumaran, V 2021 Stability and the transition to turbulence in the flow through conduits with compliant walls. *Journal of Fluid Mechanics* **924**, P1.

Landahl, Marten T 1962 On the stability of a laminar incompressible boundary layer over a flexible surface. *Journal of Fluid Mechanics* **13** (4), 609–632.

Nagy, Péter T, Szabó, András & Paal, Gyoergy 2022 The effect of spanwise and streamwise elastic coating on boundary layer transition. *Journal of Fluids and Structures* **110**, 103521.

Rosti, Marco E. & Brandt, Luca 2017 Numerical simulation of turbulent channel flow over a viscous hyper-elastic wall. *Journal of Fluid Mechanics* **830**, 708–735.

Sugiyama, Kazuyasu, Ii, Satoshi, Takeuchi, Shintaro, Takagi, Shu & Matsumoto, Yoichiro 2011 A full eulerian finite difference approach for solving fluid–structure coupling problems. *Journal of Computational Physics* **230** (3), 596–627.

Tian, Guizhong, Fan, Dongliang, Feng, Xiaoming & Zhou, Honggen 2021 Thriving artificial underwater drag-reduction materials inspired from aquatic animals: progresses and challenges. *RSC advances* **11** (6), 3399–3428.

Wang, Jin, Koley, Subhra Shankha & Katz, Joseph 2020 On the interaction of a compliant wall with a turbulent boundary layer. *Journal of Fluid Mechanics* **899**, A20.

Zhang, Cao, Miorini, Rinaldo & Katz, Joseph 2015 Integrating mach–zehnder interferometry with tpiv to measure the time-resolved deformation of a compliant wall along with the 3d velocity field in a turbulent channel flow. *Experiments in Fluids* **56**, 1–22.

Zhang, Cao, Wang, Jin, Blake, William & Katz, Joseph 2017 Deformation of a compliant wall in a turbulent channel flow. *Journal of Fluid Mechanics* **823**, 345–390.